Modular epistasis in yeast metabolism

Daniel Segrè[1], Alexander DeLuna[2], George M Church[1] & Roy Kishony[2]

Epistatic interactions, manifested in the effects of mutations on the phenotypes caused by other mutations, may help uncover the functional organization of complex biological networks[1–3]. Here, we studied system-level epistatic interactions by computing growth phenotypes of all single and double knockouts of 890 metabolic genes in *Saccharomyces cerevisiae*, using the framework of flux balance analysis[4]. A new scale for epistasis identified a distinctive trimodal distribution of these epistatic effects, allowing gene pairs to be classified as buffering, aggravating or noninteracting[2,5]. We found that the ensuing epistatic interaction network[6] could be organized hierarchically into function-enriched modules that interact with each other 'monochromatically' (*i.e.*, with purely aggravating or purely buffering epistatic links). This property extends the concept of epistasis from single genes to functional units and provides a new definition of biological modularity, which emphasizes interactions between, rather than within, functional modules. Our approach can be used to infer functional gene modules from purely phenotypic epistasis measurements.

Metabolism has been studied in its entirety, in a search for hierarchical and modular organization based on topology[7], reaction fluxes[8–10] and gene expression[11,12]. System-level organization of cellular metabolism can alternatively be explored based on the way gene mutations affect each other's phenotypic consequences. The variability spectrum of such epistatic interactions between mutations is attracting attention from the complementary perspectives of evolutionary theory and genetics[1,2,5]. From the evolutionary perspective, our understanding of many processes, including speciation, the emergence of sexual reproduction and the maintenance of genetic variability, fundamentally depends on the nature of epistasis[5,13]. Although the implications of epistasis have been studied mostly under the assumption of identical interactions between all mutations, variability in the level and 'sign' (aggravating or buffering; **Table 1**) of epistasis between different loci could substantially affect (and sometimes even reverse) its evolutionary consequences[5]. From the genetic perspective, epistatic interactions are of particular importance for elucidating functional association between genes[2,6]. This premise has motivated recent genome-wide screens for identifying pairs of synthetic-lethal mutations[1]. Such extreme aggravating interactions comprise ~0.5% of the gene pairs tested in the yeast *Saccharomyces cerevisiae* and are correlated with functional association between genes[1].

Fundamental questions remain about the distribution of the sign and magnitude of epistatic interactions for the remaining 99.5% of the gene pairs. Despite the immediate importance of these questions from both the evolutionary and the genetic perspectives, available data on the distribution of epistatic interactions are very limited. The most direct experimental measurement, analyzing fitness of double mutants in *Escherichia coli*, showed that interactions are ubiquitous and that the overall distribution of the level of interactions among random pairs of mutations is unimodal, roughly symmetric and centered near zero epistasis, despite frequent pairwise interactions[14]. This observation is supported by experimental evidence in other organisms[15–17] and by computational modeling[18,19]. Environmental factors were also suggested[19,20] and shown[21] to affect gene interactions.

Here we studied the spectrum of epistatic interactions between metabolic genes in *S. cerevisiae* using the framework of flux balance analysis (FBA), a mathematical method for computing whole-cell metabolic fluxes and growth rates based on steady-state and optimality assumptions[4,22] (**Supplementary Methods** online). Extending previous work on *in silico* yeast deletion studies, we applied FBA to the complete metabolic network of *S. cerevisiae*[4,23,24] and calculated the maximal rate of biomass production (V_{growth}) of all the networks with

Table 1 Nonscaled and scaled definitions of interactions between mutations

	Nonscaled epistasis	Scaled epistasis
	$\varepsilon = W_{XY} - W_X W_Y$	$\bar{\varepsilon} = \dfrac{W_{XY} - W_X W_Y}{\left\| \tilde{W}_{XY} - W_X W_Y \right\|^a}$
No epistasis	$\varepsilon = 0$	$\bar{\varepsilon} \approx 0$
Aggravating[b]	$\varepsilon < 0$	$\bar{\varepsilon} \approx -1$
Buffering[c]	$\varepsilon > 0$	$\bar{\varepsilon} \approx 1$

W_X and W_Y represent the fitness values of single mutants and W_{XY} represents the fitness value of the corresponding double mutant. [a]The reference fitness value is defined by

$$\tilde{W}_{XY} = \begin{cases} \min(W_X, W_Y) & \text{for } W_{XY} > W_X W_Y \\ 0 & \text{otherwise} \end{cases}.$$

[b]In evolutionary biology: synergistic epistasis, negative epistasis; in genetics: enhancers, synthetic interactions, synthetically sick. [c]In evolutionary biology: antagonistic epistasis, diminishing returns, positive epistasis; in genetics: partial suppressors, alleviating.

[1]Lipper Center for Computational Genetics and Department of Genetics, Harvard Medical School, Boston, Massachusetts 02115, USA. [2]Bauer Center for Genomics Research, Harvard University, 7 Divinity Avenue, Cambridge, Massachusetts 02138, USA. Correspondence should be addressed to R.K. (rkishony@cgr.harvard.edu).
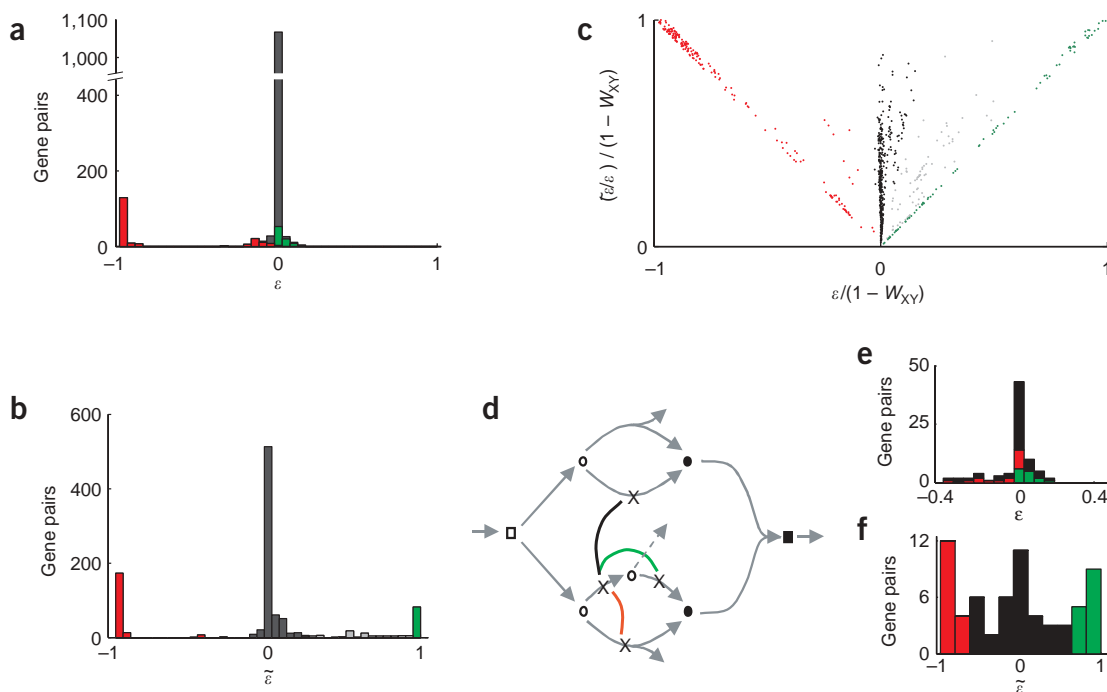
Figure 1 Epistatic interactions between mutations can be classified into three distinct classes. Fitness values of all possible double mutants relative to the expected no-epistasis values are calculated with FBA over all pairs of enzyme deletions (excluding essential genes and gene-deletions with no phenotypic consequence). The trimodal distribution is uncovered by transforming the (**a**) nonscaled epistasis level $\varepsilon = W_{XY} - W_X W_Y$ into (**b**) the new scale $\tilde{\varepsilon}$ defined in **Table 1**. The $\tilde{\varepsilon}$ values are used to classify the interactions into buffering (green) at $\tilde{\varepsilon} > \theta_+$; aggravating (red), including synthetic lethal at $\tilde{\varepsilon} = -1$ and strong synthetic sick at $\tilde{\varepsilon} < \theta_-$; and no epistasis (black). Here we used $(\theta_-, \theta_+) = (-0.25, 0.95)$. Relatively few interaction pairs (gray) fall in a nondecisive area. Although the $\tilde{\varepsilon} = 1$ point is the outermost value in the FBA model, in experimental measurements compensatory interactions could exceed this buffering case (see also **e** and **f**). (**c**) The classification of gene interactions is also evident in a scatter plot showing $\varepsilon/\tilde{\varepsilon}$ versus ε normalized to the effect of the double mutation, $1 - W_{XY}$. The ratio between the x and y axes is equal to the scaled epistasis level $\tilde{\varepsilon}$. A small random displacement was added to resolve overlapping points. (**d**) A schematic metabolic network showing simple examples of buffering, aggravating and multiplicative interactions (green, red and black arcs, respectively) between gene deletions (X). The synthesis of biomass (full square) from biomass components (full dots) requires an optimal allocation of a common nutrient (empty square) through intermediate metabolites (empty dots). Additional reactions (dotted arrow) may account for more subtle buffering interactions in the complete network (for additional details and topologies, see **Supplementary Figs. 2 and 4** online). (**e**,**f**) Distribution of epistasis in experimental data of fitness measurements of double and single mutants in RNA viruses[15]. The unimodal distribution of ε (**e**) diverges into a trimodal distribution when $\tilde{\varepsilon}$ is used (**f**). While these data support the FBA-derived trimodal distribution in the $[-1,1]$ range of $\tilde{\varepsilon}$, the presence of pairs with $\tilde{\varepsilon} > 1$ stresses the relevance of the additional class of such compensatory interactions (31 pairs, not shown). In viewing these results, one should keep in mind that, as explained in ref. 15, the data are based on a heterogeneous collection of diverse experiments and may not represent a truly random set of mutations.

single or double gene deletions relative to the rate of biomass production of the unperturbed wild-type network. For the deletion of gene X, fitness was defined as $W_X = V_{growth}^{\Delta X}/V_{growth}^{wild-type}$ (refs. 25–27). For any pair of genes X and Y, we evaluated the level of epistasis by comparing the fitness W_{XY} of the double mutant with the product of the fitness values W_X and W_Y of the corresponding single mutants[5,14,18].

We first analyzed the distribution of deviations from this multiplicative behavior using previously proposed scales (**Supplementary Fig. 1** online) and concentrated in particular on a conventional nonscaled measure of epistatic interactions: $\varepsilon = W_{XY} - W_X W_Y$ (refs. 5,14). In agreement with existing theoretical and experimental results[14,18], apart from the synthetic-lethal pairs (located at $\varepsilon \ll 0$), this approach yielded a unimodal distribution of genetic interactions centered around $\varepsilon = 0$ (**Fig. 1a**). Thus, on average, mutations in FBA combined multiplicatively to affect fitness (**Supplementary Fig. 2** online). Deviations from no epistasis towards buffering ($\varepsilon > 0$) and towards aggravating ($\varepsilon < 0$) interactions were equally common (53% and 47%, respectively). On the $\varepsilon < 0$ side of the distribution, there seemed to be a distinction between the strongly interacting synthetic-lethal pairs and other, much milder, nonlethal effects. For

$\varepsilon > 0$, however, such a distinction between strong and weak interactions was not apparent.

To assess whether a given value of ε was large or small, we used a normalization based on two natural references. For aggravating interactions, the extreme reference case was complete synthetic lethality: $W_{XY} = 0$. We compared buffering interactions to the special case in which the mutation with the stronger effect completely buffers the effect of the other mutation: $W_{XY} = \min(W_X, W_Y)$ (ref. 20). Using these reference cases, we defined a new scale, $\tilde{\varepsilon}$, which quantifies the relative strength of the interactions (**Table 1** and **Supplementary Fig. 1** online). Using the scaled measure of epistasis $\tilde{\varepsilon}$, the distribution of the epistasis level diverged into a trimodal distribution (**Fig. 1b**), which, to our knowledge, has not been previously described. Some experimental support for the predicted trimodal distribution is found in previously published fitness measurements of RNA virus mutants (**Fig. 1e,f**)[15]. The new scale $\tilde{\varepsilon}$ uncovered a qualitative distinction between different pairs of genes (**Fig. 1c**) and allowed them to be classified into three classes: buffering, aggravating and multiplicative. A schematic metabolic network demonstrating these interaction types is shown in **Figure 1d**.
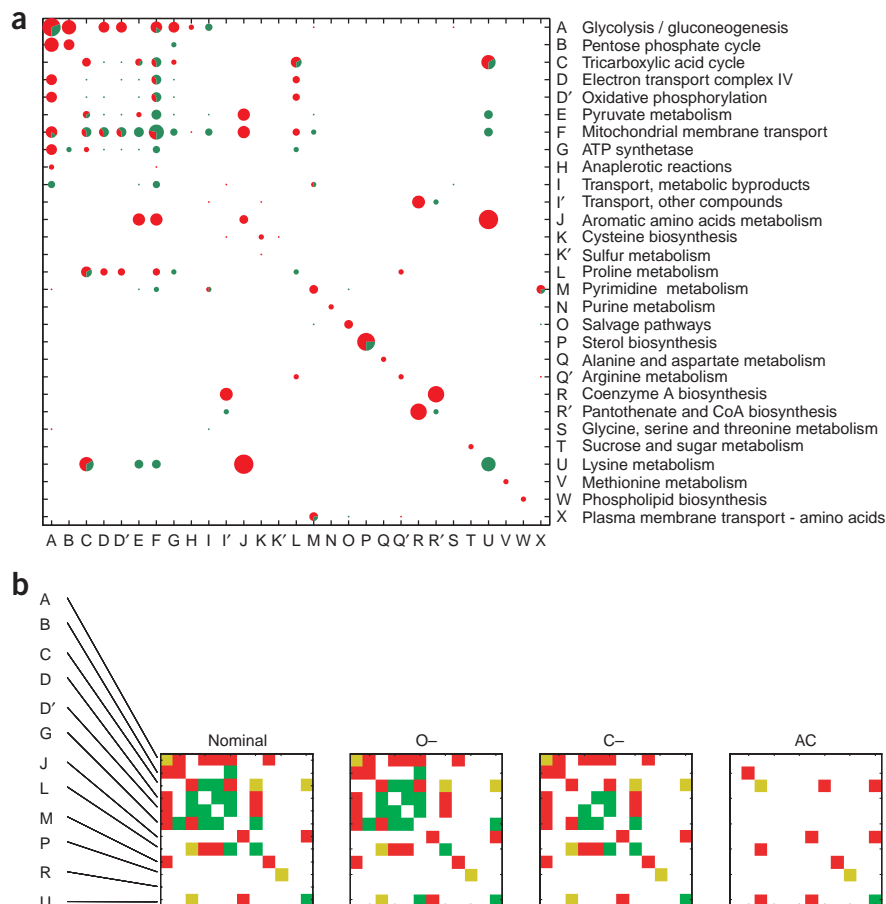
Figure 2 Epistatic interactions between genes classified by functional annotation groups tend to be of a single sign (*i.e.*, monochromatic). (**a**) Representation of the number of buffering and aggravating interactions within and between groups of genes defined by common preassigned annotation from the FBA model. The radii of the pies represent the total number of interactions (ranging logarithmically from 1 in the smallest pies to 35 in the largest). The red and green pie slices reflect the numbers of aggravating and buffering interactions, respectively. Monochromatic interactions, represented by whole green or red pies, are much more common than would be expected by chance. (**b**) Sensitivity analysis of the prevalence of monochromaticity with respect to changes in the growth conditions In each matrix, an input parameter was modified with respect to the nominal analysis: O–, 0.5× oxygen concentration; C–, 0.5× carbon concentration; AC, acetate (instead of glucose) supplied as carbon source. The color of the matrix element indicates the kind of interactions observed between the genes in different annotation groups: red for pure aggravating, green for pure buffering and yellow for mixed links. The annotation groups are represented with the same letter code used in **a** (see extended analysis in **Supplementary Fig. 3** online).

A   Glycolysis / gluconeogenesis
B   Pentose phosphate cycle
C   Tricarboxylic acid cycle
D   Electron transport complex IV
D′ Oxidative phosphorylation
E   Pyruvate metabolism
F   Mitochondrial membrane transport
G   ATP synthetase
H   Anaplerotic reactions
I   Transport, metabolic byproducts
I′ Transport, other compounds
J   Aromatic amino acids metabolism
K   Cysteine biosynthesis
K′ Sulfur metabolism
L   Proline metabolism
M   Pyrimidine metabolism
N   Purine metabolism
O   Salvage pathways
P   Sterol biosynthesis
Q   Alanine and aspartate metabolism
Q′ Arginine metabolism
R   Coenzyme A biosynthesis
R′ Pantothenate and CoA biosynthesis
S   Glycine, serine and threonine metabolism
T   Sucrose and sugar metabolism
U   Lysine metabolism
V   Methionine metabolism
W   Phospholipid biosynthesis
X   Plasma membrane transport - amino acids

This classification can be represented as a genetic network of buffering and aggravating links between genes. To understand the overall organization of the network, we started with a supervised analysis of the total number of buffering and aggravating interactions between groups of genes defined by preassigned functional annotation[23]. Pairs of epistatically interacting genes were more likely to share the same annotation than would be expected by chance (21% relative to 10% expected for random pairs, $P_{gene} \approx 10^{-11}$; **Fig. 2a**). Much additional information on functional organization, however, can be extracted by looking for patterns in the remaining 79% of the interacting gene pairs (**Fig. 2a**). These interactions tend to be either exclusively buffering or exclusively aggravating ($P_{group} < 10^{-4}$). This property, which we call 'monochromaticity' of interactions between gene sets, has a biological interpretation, and we suggest that it is an inherent part of a general definition of functional gene modules[3]. From a system-level perspective, we expect that a disruption in a given functional module (*e.g.*, a mutation affecting the synthesis of a certain amino acid) in the interaction network would either buffer or aggravate the phenotypic consequence of a disruption of a second functional module. In other words, if all the genes in a
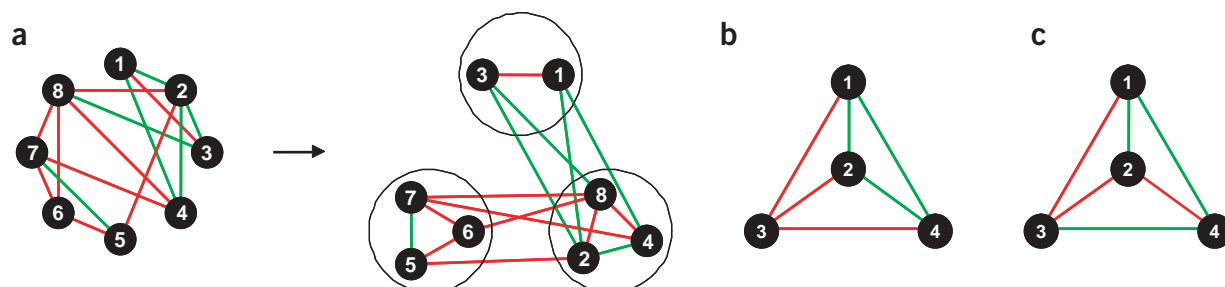

Figure 3 Schematic description of the Prism algorithm. (**a**) The algorithm arranges a network of aggravating (red) and buffering (green) interactions into modules whose genes interact with one another in a strictly monochromatic way. This classification allows a system-level description of buffering and aggravating interactions between functional modules. See also **Supplementary Video 1** online. Two networks with the same topology, but different permutations of link colors, can have different properties of monochromatic clusterability: permuting links 3–4 with 2–4 transforms a 'clusterable' graph (**b**) into a 'nonclusterable' one (**c**). See also **Supplementary Figure 6** online.
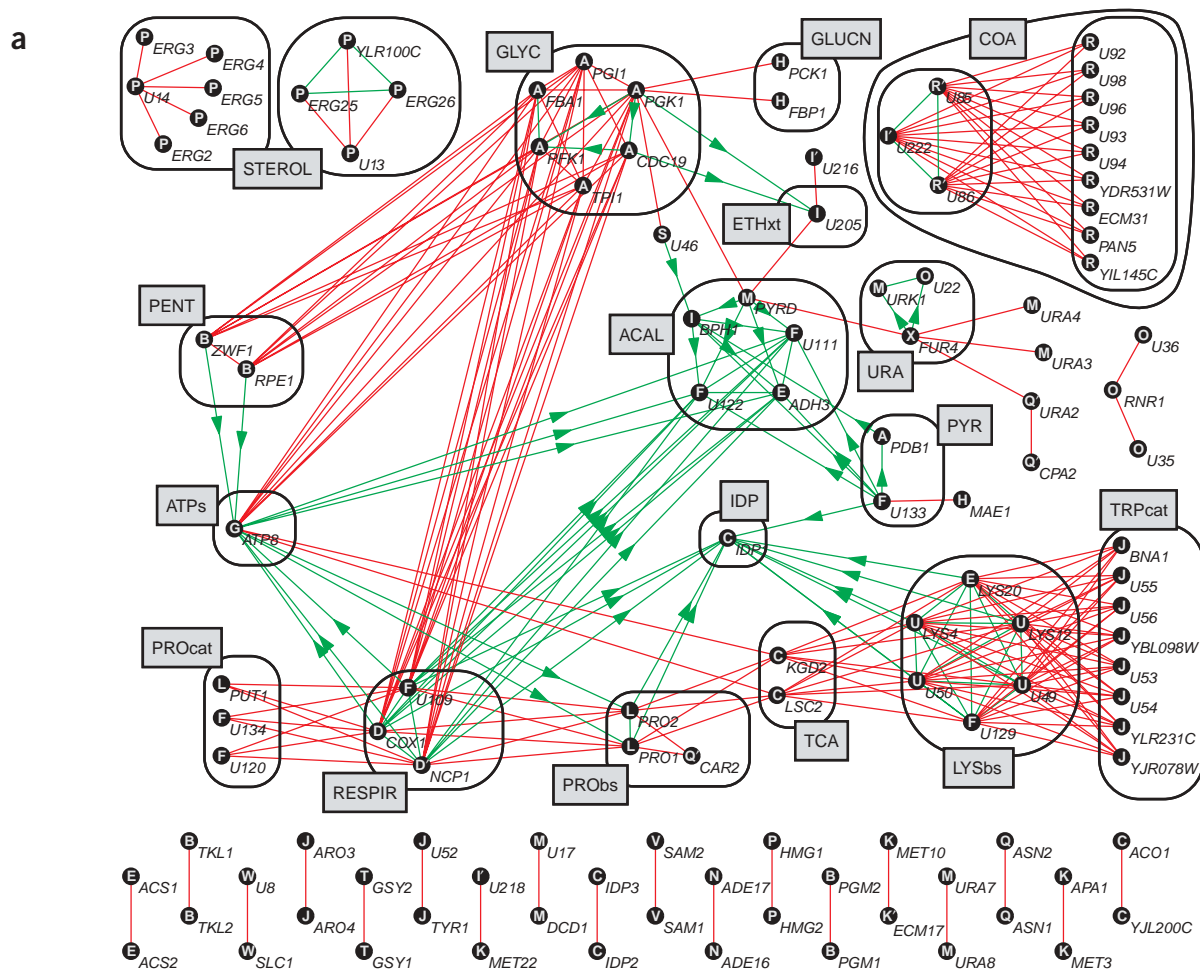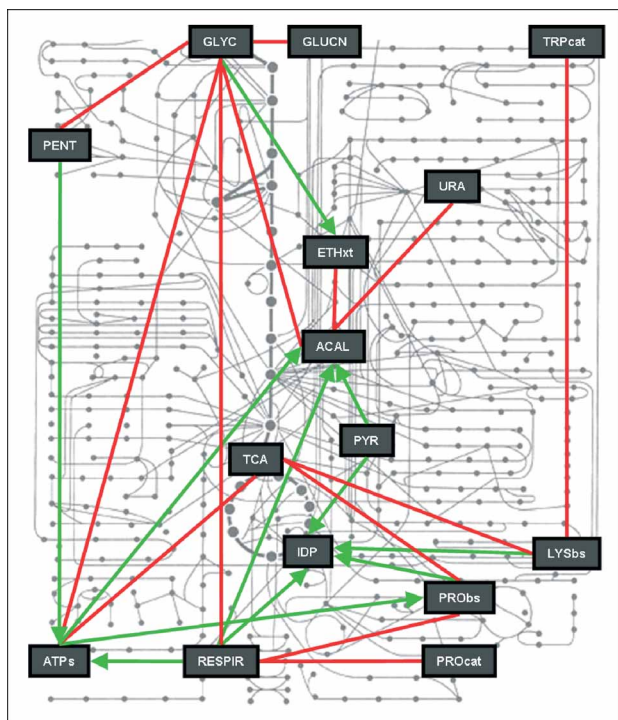
Figure 4 Unsupervised organization of the gene interaction network using the Prism algorithm. (**a**) Buffering (green) and aggravating (red) gene interaction network. Genes (black nodes) are grouped into monochromatically interacting modules (enclosing boxes). Gene annotations (white letters inside nodes; see **Fig. 2a**) correlate well with the unsupervised classification. For directional buffering links, arrows point from the deletion with the larger effect to the deletion with the smaller effect (*i.e.*, to the mutation whose fitness effect is buffered by the presence of the other; **Supplementary Fig. 4** online). Gene names are indicated on the side of the nodes. Names consisting of the letter U followed by a number correspond to enzymatic or transport reactions with unassigned genes (see URL for *S. cerevisiae* stoichiometry)[23]. Prism parameter $\alpha = 0.3$ was used. (**b**) The monochromatic organization allows a system-level view of interactions between functional modules. Notable predictions of module-module interactions include the aggravating link between LYSbs and TRPcat and the buffering one between PRObs and ATPs (for details and additional examples, see **Supplementary Note** online). 'Buffering chains', such as PENT→ATPs→PRObs→IDP, can be observed owing to the coherent directionality of the buffering links in **a**. Such chains do not necessarily have transitivity; for example, although PENT buffers ATPs, which buffers PRObs, there is no direct buffering from PENT to PRObs. The interacting functional modules are shown at their approximate locations on a schematic metabolic chart adapted from *Molecular Biology of the Cell* by B. Alberts *et al.* Reproduced by permission of Routledge/Taylor & Francis Books, Inc. Copyright 2002. Functional modules in the figure are named to reflect the main common metabolic processes of the genes involved: ACAL, acetaldehyde and acetate metabolism; ATPs, ATP synthase; COA, pantothenate and coenzyme-A biosynthesis; ETHxt, ethanol transport; GLUCN, gluconeogenesis; GLYC, glycolysis; IDP, isocitrate dehydrogenase; LYSbs, lysine biosynthesis; PENT, pentose phosphate pathway; PRObs, proline biosynthesis; PROcat, proline catabolism; PYR, pyruvate metabolism; RESPIR, respiratory chain; STEROL, sterol biosynthesis; TCA, TCA cycle; TRPcat, tryptophan catabolism; URA, uracil biosynthesis.

module are involved in the same cellular function, then the type of interaction of this module with others should not depend on the specific genes chosen in these modules. The few exceptions to monochromaticity (**Fig. 2a**) occurred mainly in annotation groups that do not overlap completely with cellular functions (*e.g.,* some tricarboxylic acid (TCA) cycle genes (group C) are involved in amino acid biosynthesis as well as in respiration; mitochondrial membrane transport genes (group F) have functions related to the different metabolites transported). Although monochromaticity was robust with respect to changes in model parameters (**Supplementary Fig. 3** online), the pattern of interactions between the modules could be substantially affected by environmental perturbations (**Fig. 2b**).

Next, we determined whether it was possible to reorganize genes into modules that had no nonmonochromatic exceptions, using an unsupervised method (*i.e.,* without taking into account existing information of gene annotation)[7,11]. Towards this goal, we developed the Prism algorithm, which hierarchically clusters interacting genes into modules that have strictly monochromatic interconnections with each other (**Fig. 3**). We found that such a classification was achievable for the entire epistasis network of yeast metabolism (**Fig. 4**) and for a wide range of parameters (**Supplementary Fig. 3** online). The probability of Prism achieving such a monochromatic classification in a random network is very small ($P_{module} < 10^{-3}$). An unbiased random search algorithm suggested that this was a consequence of an inherent mathematical property of the epistasis network, which we call 'monochromatic clusterability' (**Fig. 3b,c**). The functional modules discerned by the Prism algorithm were largely composed of genes with the same annotation (**Fig. 4a**). Genes with identical function could be grouped into the same module even in the absence of direct interaction between them (*e.g.,* PROcat and TCA modules; **Fig. 4a**). One exception was the IDP module, which did not cluster with other TCA cycle genes as expected. This is because the NADP-specific isocitrate dehydrogenase is incapable of participating in TCA cycle–based respiration but does contribute α-ketoglutarate and reduced NADPH for amino acid biosynthesis (**Supplementary Note** online). Some (63%) of the buffering links also had intrinsic directionality (**Fig. 4**), which reflects the asymmetric nature of alleviating effects that are not due to trivial buffering in the same linear pathway. The directionality was coherently organized at a high hierarchical level (**Fig. 4b**), whereas nondirectional buffering links occurred mostly in smaller modules. This emerging pattern was an unanticipated consequence of the Prism approach, rather than an input to it.

The modular organization of the epistasis network that we uncovered occurs at multiple levels. The lowest hierarchical level describes how a mutation in a given gene affects the phenotypic consequence of another mutation (**Fig. 4a**), and the highest level (**Fig. 4b**) describes how altered functionality of a given module of genes affects the phenotypic consequence of altered functionality of another module. Thus, we derived a system-level description of the network based on the new concept of epistasis between modules rather than between individual genes (**Fig. 4b**). Most of the recovered modules and their connections are in good agreement with our understanding of yeast metabolism. As expected, perturbations of the respiratory chain or the ATP synthetase would aggravate disruption of glycolysis, because either fermentation or respiratory function is needed for ATP synthesis. Similarly, respiratory chain and ATP synthetase have buffering interactions with each other, because any of these processes is indispensable for ATP synthesis through oxidative phosphorylation. On the other hand, interactions that were not expected *a priori* provide

interesting predictions of the model, which have not yet been tested in current screens[1]. For example, the simulation predicted a currently unidentified aggravating link between lysine biosynthesis and tryptophan degradation (**Supplementary Fig. 4** online). Model predictions and limitations are pointed out in **Supplementary Note** online, and an example of environment-dependent modular organization is given in **Supplementary Figure 5** online.

By measuring epistasis with respect to specific positive and negative extremes, we found a distinctive trimodal spectrum, which allowed us to define a network of buffering and aggravating gene interactions. The resulting genetic interaction network identified a special organization of genes into modules that interact with each other through exclusively buffering or exclusively aggravating links. This concept of monochromatic modularity extends the classical gene-gene definition of epistasis to the level of functional units. These results suggest a new definition of biological modularity, which emphasizes interconnections between modules and could complement approaches emphasizing intramodule properties[28]. It will be interesting to explore what correspondences exist between gene associations identified using different classical and modern conceptual approaches[7–12,28–30]. In particular, modules defined through monochromatic epistatic interactions may be reflected in gene cotranscription patterns[11] or in covariation of module components at other levels[30]. The trimodal spectrum we predicted computationally, which is also observed in experimental data[15], could replace a commonly used hypothesis of identical interactions between all mutations for addressing specific fundamental questions in evolution, such as the possible advantage of sexual reproduction in purging deleterious mutations[5,13]. Complementing our sensitivity analysis, it would be interesting to study the universality of this trimodal distribution with respect to different assumptions and models, such as different environmental conditions[24], objective functions[22] and deviation from optimality[27]. Most notably, future large-scale experimental measurements of epistatic interactions could be designed to test the predicted distribution. Unlike synthetic-lethal screens, characterization of buffering interactions inherently requires much more accurate phenotypic fitness measurements of single and double mutants. Although the FBA model has been valuable in our preliminary exploration of system-level organization of epistasis networks, our current results are specific to computational predictions in deleterious metabolic enzyme knockouts. Quite different patterns might emerge in other types of epistatic interaction, such as those involving beneficial mutations, partial loss of function, regulatory genes or multicellular developmental networks. New types of interactions, such as the compensating interactions discernible in the RNA-virus data set, may motivate the extension of our monochromatic classification approach to networks with more than two colors. Monochromaticity could also be extended to other types of networks in which multiple kinds of mutually exclusive interactions are present, as well as to directed networks, where unidirectional interacting modules could be defined.

METHODS

FBA. In FBA, mass conservation and additional simplifying assumptions are used to produce quantitative predictions of steady-state rates of metabolic reactions (or fluxes; V_i, $i = 1,…,N$). FBA has been described in detail elsewhere[4] (see **Supplementary Methods** and **Supplementary Table 1** online for a list of FBA parameters). The two fundamental steps in FBA are (i) the use of linear constraints to define a space Φ of feasible reaction fluxes for the network and (ii) an optimization step, aimed at finding the set of fluxes in Φ that maximize a given linear objective function, using linear programming. The

major set of constraints (mass conservation) can be written as $\Sigma S_{ij}V_j = 0$, where S_{ij} is the stoichiometric coefficient of metabolite M_i in reaction j. Our S matrix also incorporates stoichiometric information about all exchange reactions (uptake and secretion) and about the maintenance and growth reactions. The growth reaction, $\Sigma c_i M_i \to$ biomass, is based on measured organism-specific biomass composition (the c_i coefficients). Its flux V_{growth} is the objective function to be maximized. Lower and upper bounds for fluxes ($a_j \le V_j \le b_j$) are used to impose irreversibility of certain reactions, to define nutrient uptake limitations and to impose the range or value of the maintenance flux. The specific *S. cerevisiae* stoichiometric model used in this analysis is based on a recently published reconstruction[23] (see URLs and **Supplementary Methods** online). Our nominal simulated setting consists of a $\Delta his3$ $\Delta leu2$ $\Delta rip1$ strain grown on glucose and oxygen-limited minimal medium containing nitrogen, phosphate, sulfate, threonine, histidine, leucine and uracil. Sensitivity with respect to the main condition-specific parameters is studied in **Supplementary Figure 3** online.

Double mutants and epistatic network. Complete deletions of metabolic genes are handled in FBA by setting the corresponding fluxes to zero. Evidence of substantial agreement between experimental data and the FBA predictions for viability of yeast single mutants has been shown[4,24] (**Supplementary Methods** online). Fitness for the mutant of gene X is defined as

$$W_X = \frac{\max_V\{V_{growth}|V \in \Phi, V_X = 0\}}{\max_V\{V_{growth}|V \in \Phi\}}.$$

Like the fitness used in ref. 26, the FBA fitness used here is defined as the mutant growth rate normalized to the wild-type one and is a function of the fluxes of the major carbon utilization pathways. For double mutants, the new constraints are added for both deleted genes. Some caution is required for isoenzymes, as well as in cases where the enzyme is a protein multimer. Also, some genes encode enzymes that catalyze more than one reaction. Such cases are treated by appropriately keeping track of gene-enzyme-flux relationships. We carried out the computations using the commercial software Xpress. A typical run of all the double mutants took ~ 1 d on a single Pentium 4 processor. After carrying out the FBA double mutant calculations, we calculated the matrix of scaled epistasis $\tilde{\varepsilon}_{X,Y}$ between gene pairs (X,Y) ($X,Y = 1,\ldots,N$ genes; **Table 1**). The epistasis network, $E_{X,Y}$, is then defined as a discretization of the $\tilde{\varepsilon}_{X,Y}$ values based on two cutoff parameters, θ_- and θ_+: $E_{X,Y} = -1$ if $\tilde{\varepsilon}_{X,Y} < \theta_-$; $E_{X,Y} = 1$ if $\tilde{\varepsilon}_{X,Y} > \theta_+$; and $E_{X,Y} = 0$ otherwise. We used noise cutoff as described in **Supplementary Table 1** online. Sensitivity with respect to θ_- and θ_+ and the noise cutoff parameters is shown in **Supplementary Figure 3** online.

The Prism algorithm. The algorithm for pairwise reduction into subgraphs monochromatically (Prism) carries out agglomerative clustering, with the additional feature of avoiding, when possible, the generation of clusters that do not interact with each other monochromatically (**Supplementary Fig. 6** online). At the onset, each gene is assigned to a distinct cluster. In sequential clustering steps, pairs of clusters are combined until the whole network is covered. At each step, the biological proximity, or affinity $A_{x,y}$ between cluster x (size n_x) and cluster y (size n_y), is computed as the linear combination $A_{x,y} = \alpha A^d_{x,y} + (1 - \alpha)A^a_{x,y}$ of a direct affinity

$$A^d_{x,y} = \sum_{X \in x, Y \in y} |E_{X,Y}|/(n_x n_y)$$

and an associative affinity

$$A^a_{x,y} = \max_{X \in x, Y \in y}\{a^\gamma_{X,Y}\}$$

(single linkage), where

$$a_{X,Y} = 1 - \sum_{Z=1}^N |E_{X,Z} - E_{Y,Z}|/(2N).$$

At every step, each cluster pair (x,y) is also assigned an integer $C_{x,y}$, counting how many nonmonochromatic connections would be formed if clusters x and y

were joined (*i.e.*, the number of clusters z that have buffering links with x and aggravating links with y, or vice versa). The algorithm hence identifies the set ψ of (x,y) pairs for which $C_{x,y} = C_m$, where

$$C_m = \min_{x,y}\{C_{x,y}\}.$$

The set ψ contains all the candidate pairs that, if joined at the next step, would cause the minimal possible number of monochromatic conflicts. The pair with highest $A_{x,y}$ in ψ is then chosen as the pair of clusters to be combined. At a given step, monochromaticity is preserved if $C_m = 0$. The final clustering solution is assigned a total module-module monochromaticity violation number, $Q_{module} = \sum C_m$, where the sum is over all the clustering steps. For sensitivity of Prism with respect to choice of parameters α and γ, see **Supplementary Figure 3** online.

Prism carries out a greedy classification, based both on monochromaticity and on the biological relatedness embodied in the affinities. We also implemented a variant, Prism-R, aimed at evaluating the monochromatic clusterability of a network (*i.e.*, how likely it is to find monochromatic solutions in a given network). Prism-R works similarly to Prism, except it ignores the affinities and chooses at random from ψ the pair of clusters to be combined at each step. Multiple runs of Prism-R on a given network may result in different numbers of monochromatic violations, Q_{module}. For a given network, the average number of monochromatic violations over an ensemble of Prism-R clustering solutions is defined as $Q_{cluster} = \langle Q_{module} \rangle$. In the calculations presented, we used an ensemble of 100 Prism-R runs for each network tested. A Matlab implementation of Prism and Prism-R is available on the authors' website (see URLs).

Enrichment for annotation similarity between interacting genes. This test assesses the statistical significance of the enrichment of common functional annotation among pairs of interacting (either buffering or aggravating) genes versus what would be expected by chance. Our null hypothesis is that the true enrichment is the one expected if gene interactions were assigned at random. In a one-tailed test, the P value can be computed as the probability of randomly observing a subset of at least k interacting pairs with identical annotation from a set of size n of interacting pairs (with a total of K same-annotation pairs in the full set of N pairs), given by the hypergeometric distribution,

$$P_{gene} = 1 - \sum_{i=0}^{k-1} \binom{K}{i}\binom{N-K}{n-i}\Big/\binom{N}{n}.$$

The N gene pairs do not include essential genes and gene deletions without phenotypic consequence. For the nominal conditions (**Supplementary Methods** online), of a total number $n = 278$ of interacting gene pairs, 21% have identical annotation (*i.e.*, $k = 59$ pairs), compared with 10% ($K = 104$) among all $N = 1,034$ gene pairs. The resulting P value is $P_{gene} \approx 10^{-11}$, which suggests that our null hypothesis is not true.

Significance level of monochromatic interactions in the annotation groups. A pair of annotation groups G_1 and G_2 is defined as violating monochromaticity if there are both buffering and aggravating epistatic links connecting genes in G_1 with genes in G_2. We define Q_{group} as the number of pairs of annotation groups that violate monochromaticity. Having found for the yeast epistatic network that $Q_{group} = 9$ (**Fig. 2a**), we wanted to know whether this corresponded to an enrichment of monochromatic interactions in a statistically significant way. Our null hypothesis was that Q_{group} is what would be expected for a random network. To test this hypothesis, we carried out 10,000 randomizations of the networks, in which the annotation and the topology of gene-gene interactions were conserved but the sign (buffering or aggravating) of each link was randomly assigned (**Supplementary Fig. 7** online). The total numbers of buffering and aggravating interactions were fixed. We computed Q_{group} for each of these randomized networks and compared the resulting distribution with the observed value (**Supplementary Fig. 7** online). None of the 10,000 random networks had fewer mixed links than the real network, corresponding to an upper bound for the P value of $P_{group} < 10^{-4}$. This is a conservative estimate (**Supplementary Fig. 7** online), as quantified by the number of standard deviations ($Z_{groups} = 9.7$) separating the observed value ($Q_{group} = 9$) and the average of the distribution (24.5 ± 1.6).

Significance level for monochromatic clusterability by Prism. The Prism algorithm, when applied to the epistasis interaction network of yeast metabolism, yields a fully monochromatic solution (*i.e.*, $Q_{module} = 0$). Here we tested the null hypothesis that the true Q_{module} is the one expected for a randomized network. We applied the Prism algorithm to 1,000 networks that were randomized as explained above and in **Supplementary Figure 7** online. For each network, we calculated the number of monochromatic violations, Q_{module}. For the real network we had $Q_{module} = 0$, whereas for all the randomized networks we found $Q_{module} > 0$ ($Q_{module} = 7.73 \pm 1.5$; **Supplementary Fig. 7** online); hence, $P_{module} < 10^{-3}$. This result is based on Prism and is algorithm-dependent.

A probabilistic test for monochromatic clusterability. We carried out a less biased probabilistic test for monochromatic clusterability (which is not constrained by affinities $A_{x,y}$) by calculating $Q_{cluster}$ using Prism-R for each of the 1,000 randomized networks defined above. We tested the null hypothesis that the true $Q_{cluster}$ is the one expected for a randomized network. None of the randomized networks had a lower value of $Q_{cluster}$ than the real network ($P_{cluster} < 10^{-3}$). The value of $Q_{cluster}$ in the random networks was 12.9 ± 0.43, compared with 2.73 in the real network (**Supplementary Fig. 7** online). We obtained a similar significance level (data not shown) with a different randomization of the network, which allowed for varying topologies while preserving the degree distribution of buffering and aggravating links per node[28] (**Supplementary Fig. 7** online).

URLs. The *S. cerevisiae* stoichiometric reconstruction[23] and other details relevant for building the FBA model can be found at http://www.genome.org/cgi/content/full/13/2/244/DC1/. Additional model details and the Prism algorithm are available at http://www.cgr.harvard.edu/kishony/prism/. Gene knockout fitness data calculated in this work can be downloaded from ftp://ftp.ebi.ac.uk/pub/databases/FBA2KO.

1. Tong, A.H.Y. *et al.* Global mapping of the yeast genetic interaction network. *Science* **303**, 808–813 (2004).
2. Hartman, J.L., Garvik, B. & Hartwell, L. Cell biology - Principles for the buffering of genetic variation. *Science* **291**, 1001–1004 (2001).
3. Hartwell, L.H., Hopfield, J.J., Leibler, S. & Murray, A.W. From molecular to modular cell biology. *Nature* **402**, C47–C52 (1999).
4. Famili, I., Forster, J., Nielsen, J. & Palsson, B.O. Saccharomyces cerevisiae phenotypes can be predicted by using constraint-based analysis of a genome-scale reconstructed metabolic network. *Proc. Natl. Acad. Sci. USA* **100**, 13134–13139 (2003).
5. Phillips, P.C., Otto, S.P. & Whitlock, M.C. *Beyond the Average: The Evolutionary Importance of Gene Interactions and Variablity of Epistatic Effects. in Epistasis and the Evolutionary Process* (eds. Wolf, J.B., Brodie III, E.D. & Wade, M.J.) 20–38 (Oxford University Press, New York, 2000).
6. Anholt, R.R. *et al.* The genetic architecture of odor-guided behavior in Drosophila: epistasis and the transcriptome. *Nat. Genet.* **35**, 180–184 (2003).
7. Ravasz, E., Somera, A.L., Mongru, D.A., Oltvai, Z.N. & Barabasi, A.L. Hierarchical organization of modularity in metabolic networks. *Science* **297**, 1551–1555 (2002).
8. Almaas, E., Kovacs, B., Vicsek, T., Oltvai, Z.N. & Barabasi, A.L. Global organization of metabolic fluxes in the bacterium Escherichia coli. *Nature* **427**, 839–843 (2004).
9. Papin, J.A., Reed, J.L. & Palsson, B.O. Hierarchical thinking in network biology: the unbiased modularization of biochemical networks. *Trends Biochem. Sci.* **29**, 641–647 (2004).
10. Klamt, S. & Gilles, E.D. Minimal cut sets in biochemical reaction networks. *Bioinformatics* **20**, 226–234 (2004).
11. Ihmels, J., Levy, R. & Barkai, N. Principles of transcriptional control in the metabolic network of Saccharomyces cerevisiae. *Nat. Biotechnol.* **22**, 86–92 (2004).
12. Segal, E. *et al.* Module networks: identifying regulatory modules and their condition-specific regulators from gene expression data. *Nat. Genet.* **34**, 166–176 (2003).
13. Kondrashov, A.S. Deleterious Mutations and the Evolution of Sexual Reproduction. *Nature* **336**, 435–440 (1988).
14. Elena, S.F. & Lenski, R.E. Test of synergistic interactions among deleterious mutations in bacteria. *Nature* **390**, 395–398 (1997).
15. Burch, C.L., Turner, P.E. & Hanley, K.A. Patterns of epistasis in RNA viruses: a review of the evidence from vaccine design. *J. Evol. Biol.* **16**, 1223–1235 (2003).
16. Elena, S.F. Little evidence for synergism among deleterious mutations in a nonsegmented RNA virus. *J. Mol. Evol.* **49**, 703–707 (1999).
17. Wloch, D.M., Borts, R.H. & Korona, R. Epistatic interactions of spontaneous mutations in haploid strains of the yeast Saccharomyces cerevisiae. *J. Evol. Biol.* **14**, 310–316 (2001).
18. Lenski, R.E., Ofria, C., Collier, T.C. & Adami, C. Genome complexity, robustness and genetic interactions in digital organisms. *Nature* **400**, 661–664 (1999).
19. You, L.C. & Yin, J. Dependence of epistasis on environment and mutation severity as revealed by in silico mutagenesis of phage T7. *Genetics* **160**, 1273–1281 (2002).
20. Kishony, R. & Leibler, S. Environmental stresses can alleviate the average deleterious effect of mutations. *J. Biol.* **2**, 14 (2003).
21. Remold, S.K. & Lenski, R.E. Pervasive joint influence of epistasis and plasticity on mutational effects in Escherichia coli. *Nat. Genet.* **36**, 423–426 (2004).
22. Kauffman, K.J., Prakash, P. & Edwards, J.S. Advances in flux balance analysis. *Curr. Opin. Biotechnol.* **14**, 491–496 (2003).
23. Forster, J., Famili, I., Fu, P., Palsson, B.O. & Nielsen, J. Genome-scale reconstruction of the Saccharomyces cerevisiae metabolic network. *Genome Res.* **13**, 244–253 (2003).
24. Papp, B., Pal, C. & Hurst, L.D. Metabolic network analysis of the causes and evolution of enzyme dispensability in yeast. *Nature* **429**, 661–664 (2004).
25. Fong, S.S. & Palsson, B.O. Metabolic gene-deletion strains of Escherichia coli evolve to computationally predicted growth phenotypes. *Nat. Genet.* **36**, 1056–1058 (2004).
26. Dykhuizen, D.E., Dean, A.M. & Hartl, D.L. Metabolic flux and fitness. *Genetics* **115**, 25–31 (1987).
27. Segrè, D., Vitkup, D. & Church, G.M. Analysis of optimality in natural and perturbed metabolic networks. *Proc. Natl. Acad. Sci. USA* **99**, 15112–15117 (2002).
28. Milo, R. *et al.* Network motifs: simple building blocks of complex networks. *Science* **298**, 824–827 (2002).
29. Kaufman, A., Kupiec, M. & Ruppin, E. Multi-knockout genetic network analysis: the Rad6 example. in *2004 IEEE Computational Systems Bioinformatics Conference* 332–340 (IEEE, Stanford, California, 2004).
30. Salthe, S.N. Evolving Hierarchical Systems. (Columbia University Press, New York, 1985).